Analysis of an X-Y Scanner Magnet for Use in Cancer Radio Therapy Treatment

Jackson P. Morgan
Lee Teng Undergraduate Fellowship
Oregon Institute of Technology; 3201 Campus Dr; Klamath Falls, OR 97601

Dr. Brahim Mustapha Ph.D.
Physics Division
Argonne National Laboratory; 2300 Cass Ave; Lemont, IL 60439

August 23rd, 2019

ABSTRACT

A new Carbon Ion cancer therapy center has been proposed at Argonne National Lab. This system would need a scanner magnet to be able to steer the beam into a 40cm X 40cm square which will enable it to cover all tumor sizes and shapes. This action coupled with the deposition nature of charged particles (Bragg Peak feature) and the ability to vary the energy from a linear accelerator will enable for 3D "painting" of a tumor and less collateral damage to surrounding healthy tissue. Such a magnet has been designed and the focus of this project was to perform magnetic analysis. Through CST 3D analysis it has been found that DC losses will be 155kW and AC peak losses within the conductors operating at their required AC currents will be about 250 kW while suppressing the magnet field by about 20%.

INTRODUCTION

One of the most common ways to treat a cancerous tumor within the human body is to irradiate it using x-rays. A high intensity dose of high-energy photons is shot through the patient towards the tumor. These rays cannot be targeted to terminate at any depth within a patient meaning that collateral damage might be imparted on surrounding tissue. This leads to increase chance of cancerous tumors breaking out in that tissue in the future as well as causes the patient significant discomfort.

Protons can be accelerated and used to target these tumors in depth as they produce a feature known as Bragg Peak. This peak can be targeted using varying energies to avoid surrounding tissue. Further accuracy and precision can be achieved using heavy ions as their Bragg Peaks are sharper with less scattering than protons, and therefore lead to a more compact dose of radiation. Figure 1, at right, shows this relationship where dose is plotted vs. depth.

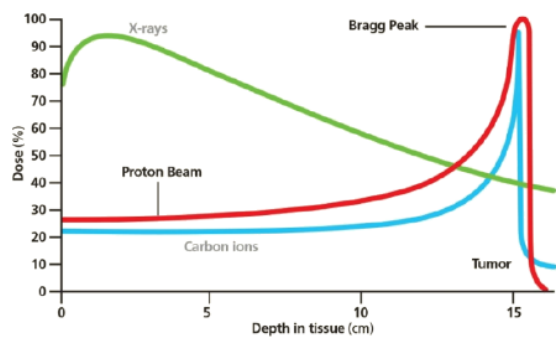

Figure 1. Showing the formation of the Bragg Peak [4].

MAGNET SPECIFICATIONS & REQUIREMENTS

A carbon ion machine, which if built will be the first of its kind in the country, has been proposed at Argonne National Lab and will require a device known as an X-Y scanner magnet [1] to be placed on the end. This device will target the tumor in the X-Y plane while the accelerating structure varies the energy of the ions, which will scan the Z depth, enabling a 3D painting of the tumor.

The following were the initial design specifications, and were determined pervious to the beginning of this project, whose primary goal will be the quantification of the magnetic field and power losses in the AC regime.

Parameter	X Value	Y Value
Scanning field	40 cm	40 cm
Scanning frequency	100 Hz	10 Hz
Full magnet aperture	6 cm	6 cm
Total magnet length	60 cm	60 cm
Field Integral – BL	0.5 Tm	0.5 Tm
Iron Thickness	6 cm	6 cm
Iron Lamination	0.25 mm	0.25 mm

Table 1. Magnet requirements.

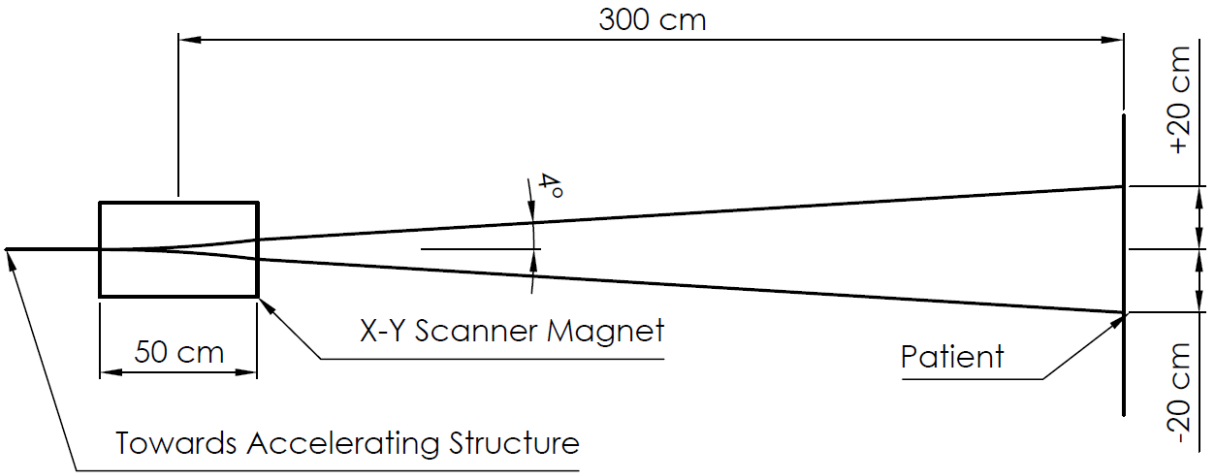

Figure 2. The X-Y scanner magnet in relation to the patient.

ANALYTICAL CALCULATIONS

Calculations were done in order to gain a general idea of power losses the magnet would experience. The following is the resistive losses and was derived from the definition of electrical power and resistivity.

$$P_{DC}\left[\frac{W}{Cond}\right] = I^2 \frac{\rho * L_{EFF}}{A} \tag{1}$$

Where:

ρ [Ωm] = Electrical resistivity of the conductor (Copper ≅1.78×10^{-8})

A [m^2] = Cross sectional area of the conductor.

L_{EFF} [m] = Effective length of the coils

I [A] = Peak current within the conductors

Parameter	Horizontal (10Hz)	Vertical (100Hz)
A [m^2]	0.0001	0.0001
I [A]	2300	2300
# Of Conductors	108	72
Effective Length [m]	0.9349	0.9349
Total Power Loss [kW] (eq. 1)	95.1	63.4

Table 2. Calculations for DC power losses within the coils.

Also, calculations were done to gain a preliminary idea of the losses within the conductors operating in an alternating current. The formula below makes the assumption that magnetic flux density will not change drastically in the AC regime vs. the DC [2].

$$P_{AC}\left[\frac{W}{Cond * m}\right] = \frac{\omega^2 B^2 A\, a^2}{12\, \rho} \tag{2}$$

Where:

ω [rad/s]= Angular frequency of the source current.

B [T] = Maximum value along field at center of magnet.

a [m] = width of conductor.

Parameter	Horizontal (10Hz)	Vertical (100Hz)
ω [rad/s]	20π	200π
B_{PEAK} [T]	0.6	0.5
A [m^2]	0.0001	0.0001
a [m]	0.01	0.01
# Of Conductors	108	72
Effective Length [m]	0.9349	0.9349
Total Power Loss [kW] (eq. 2)	16.2	852

Table 3. Calculations for AC power losses in the coils.

Knowing that the resistive losses should be around 159 kW and the AC losses should be around 868 kW we can move forward with a first estimate to compare our untested models against.

MODELING & RESULTS

Modeling and computational analysis was primarily done in CST 3D Studio Suite with conformational models being produced in CST 2D and FEMM (Finite Element Method Magnetics, which is a free 2D FEA E&M field solver [3]). CST 2D is available for both the Magnetostatic Solver and the Low Frequency Time Domain (Not available in the LF frequency domain) and is a far quicker method of calculating magnetic fields vs the 3D.

MAGNETOSTATIC

Magnetostatic modeling was done to confirm results with analytical calculations, initialize the models, confirm their status as working in the simpler static domain, and to gain a baseline agreement between the various solvers and programs used to model the magnet.

Three models were generated, one using the idealized *coil generation* option within CST, another using that option but generating a new coil for each individual strand that the magnet would contain, and finally a magnet created using the *sweep* option within CST to model real conductors that will interact with eddy currents and have resistive losses. These are called the idealized, idealized stranded, and the real respectively. The real model was the primary goal of analysis as it could be used later in the low frequency domain to attain total losses due to alternating current operations.

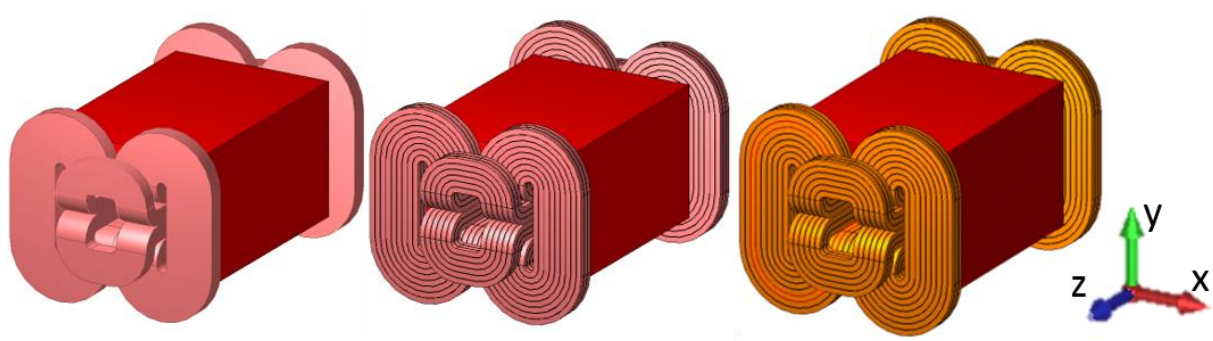

Figure 3. Three static 3D models produced including the idealized (right), idealized stranded (middle) and the real (left).

With these models we were able to solve all three to produce matching field profile curves in for both $B_x(z)$ and $B_y(z)$ (see Figure 5) with matching maxima. This gave us confidence in our primary model of choice to use, the real. The following charts and table display these results ascertained from the 3D CST models. The

real conductor is the only model that was able to produce an answer for resistive losses as the other two are modeled as perfect conductors (thus idealized).

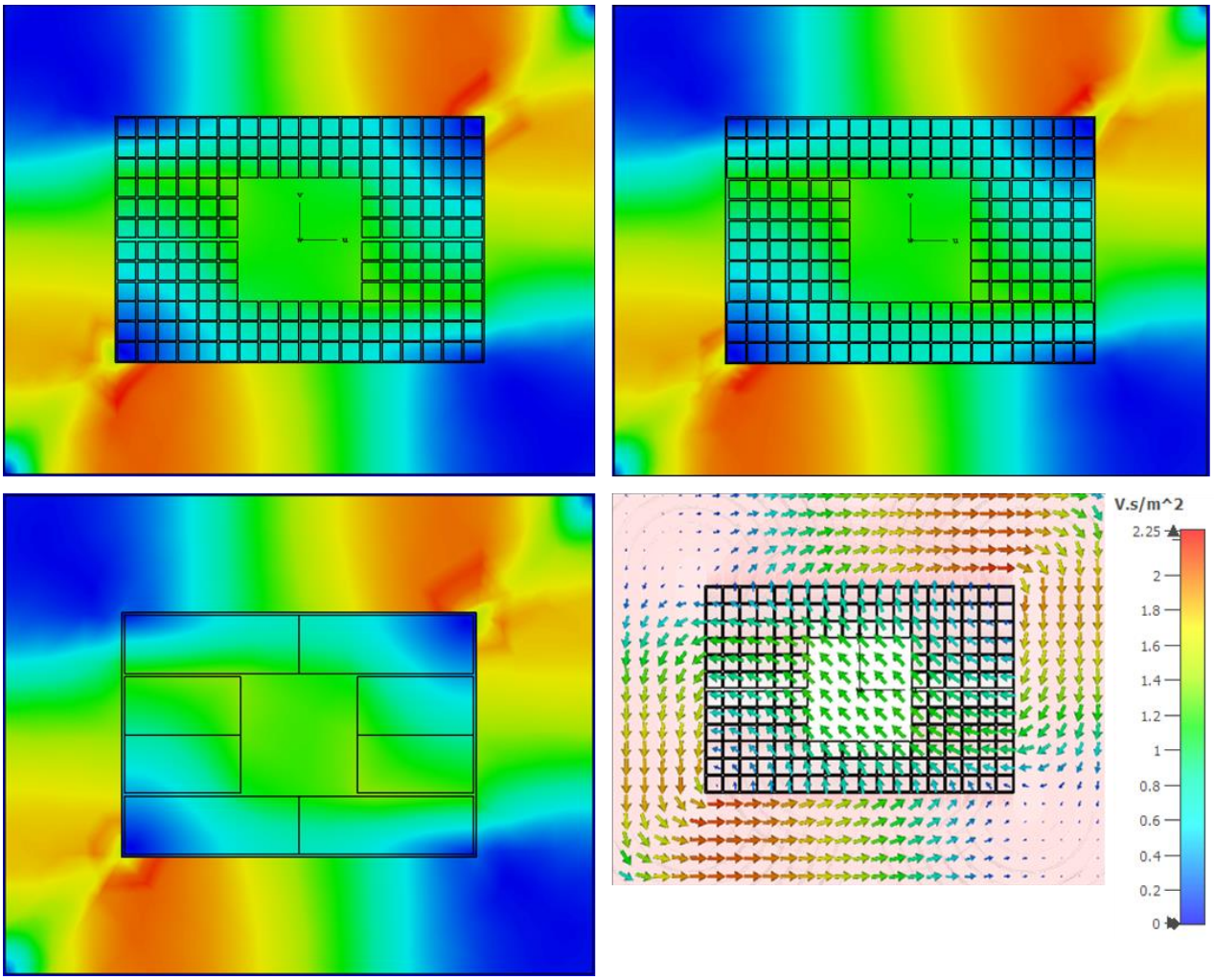

Figure 4. Showing the results of the B-field after the static solver as displayed on a contour plot at the z=0 cut plane with the real (top left), idealized stranded (top right), idealized (bottom left) and a vector plot of the real to show directionality (bottom right).

The images in Figure 4 show the pattern within all three models and demonstrate the development of spiking field around the bottom left and top right areas within the iron. This can be explained by the vector plot in Figure 4 (bottom left) which shows the directionality of the field. The field has to make a tight corner around the iron causing the flux to spike dramatically.

Result	Idealized	Idealized Stranded	Real
$B_x(0,0,0)$ [T]	0.854	0.781	0.785
$B_y(0,0,0)$ [T]	0.892	0.839	0.835
Total Losses [kW]	N/A	N/A	154.22 kW
B_x (B_y) Field Integral [Tcm]	47.9 (48.9)	43.7 (45.8)	43.7 (45.4)
B_x (B_y) Total Magnetic Length [cm]	56.1 (54.8)	56.0 (54.6)	56.0 (54.4)

Table 4. Results of various 3D CST models after static analysis.

The value for total losses for the real conductor is almost exactly what we had estimated with analytical calculations (that value being 159 kW). This increases confidence in these models to yield viable results. Furthermore, we see good agreement in field distribution between all three models and almost identical results from the two stranded models.

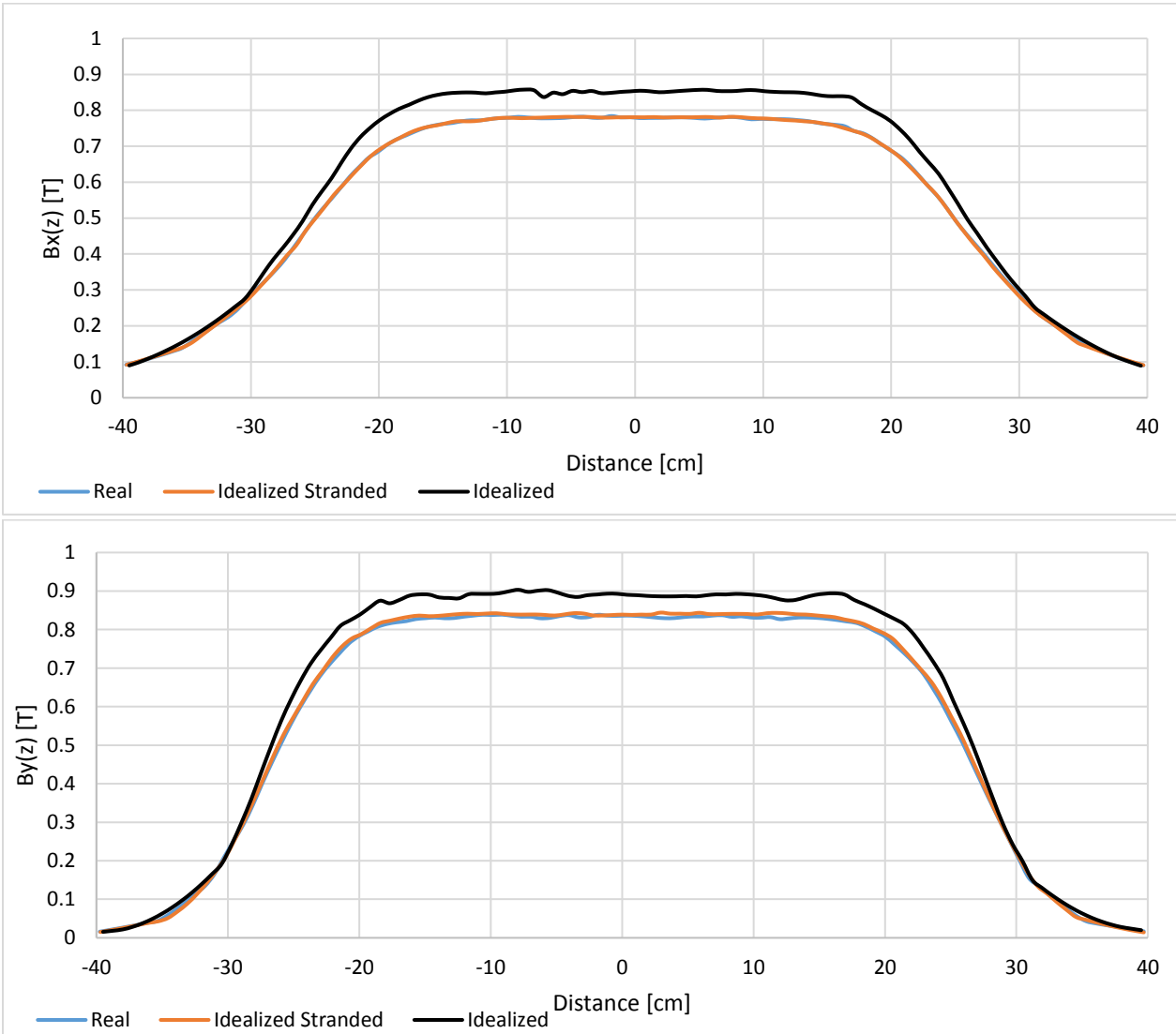

Figure 5. Bx(z) (Top) and By(z) (Bottom) plotted through each static model.

Figure 5 demonstrates the matching profile and amplitude between the two models where the empty space reserved for insulation between conductors is taken into account and with the non-stranded model increasing in amplitude while maintaining the profile. This shows that the spacing in-between conductors will slightly suppress the field. This is not an issue as there is ability for current to be increased thus raising the profiles.

Conformation Modeling

This modeling was done in CST 2D (planar mesh) as well as in FEMM and is exclusively analyzed in 2 dimensions.

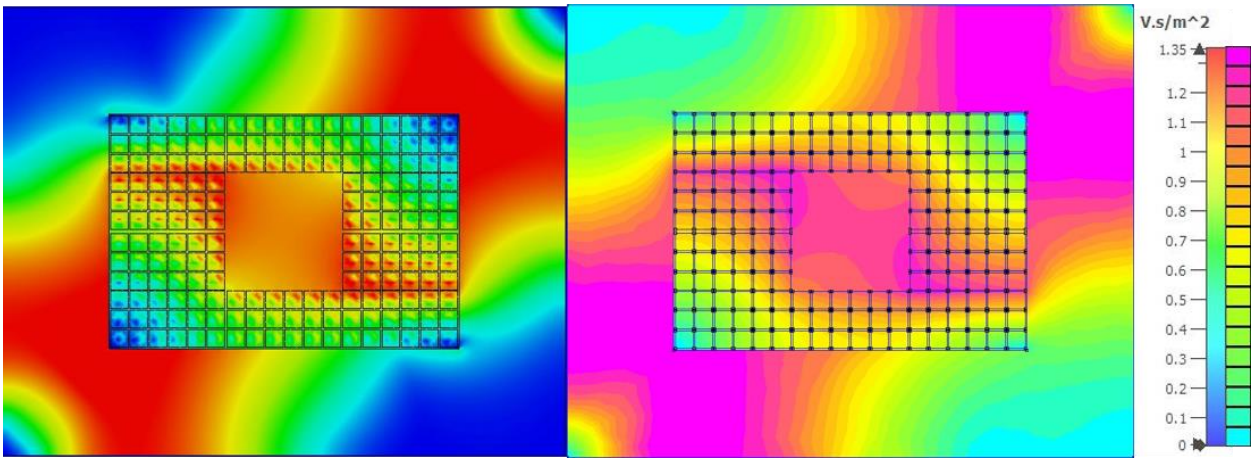

Figure 6. CST 2D (right) and FEMM (left) contour plots of B-field at the z=0 cross-section.

Figure 6 shows complete agreement between both of these 2D analytical methods and overall the same patterns as in the 3D models. The primary difference is in the magnitude of B-field within the iron. If the respective scales are examined it can be found that there are far more significant maxima in the 3D calculation than the 2D. It is believed that these differences are due to the nature of the 2D models themselves, not taking into account the alterations in the field that might be seen in the 3rd dimension due to things like end effects.

Parameter	Real (3D Model)	FEMM (2D)
$B_x(0,0,0)$ [T]	0.785	0.786
$B_y(0,0,0)$ [T]	0.835	0.847
B_{PEAK} [T] (at z=0 cut plane)	2.223	1.345

Table 5. Results from 2D compared to that of 3D analysis.

FEMM produces a given amount of losses per unit length. When multiplied by the effective length the value comes out to 155 kW. An exact conformation of the resistive losses within the coils found in 3D models and in the analytical calculations.

LOW FREQUENCY ANALYSIS

After a long period of trial and error with various modeling techniques, it was found that the utilization of current paths, defined on slices in the coil ends (ears), would yield viable results within the low frequency, frequency domain (LFFD) solver. Also, it was found that if low meshing parameters were used, the B-field through the center of the magnet along the z-direction would be invalid, as it would alter both the field profile and amplitude. This means that high meshing values were needed to produce viable results.

The real model was the primary one worked on within the LFFD domain as it has the ability to find the eddy losses within the coil. Also when reliable results were found at a given mesh setting the idealized stranded model, was used to confirm those results through comparison of the B-field.

As all these operations were done within the frequency domain where only one frequency could be simulated at a time. Different models were made for the magnet. One at 10 Hz where the current in the Y-(100 Hz)-coil would be turned off, and one with complementary parameters. Further modeling was also done in the low frequency time domain (LFTD) solver, where two different frequencies could be established and run concurrently, to increase confidence in the model. The reason this was not used over the course of all modeling is due to the incredible length of time it takes to calculate anything within the

LFTD, issues with computer hardware not being able to run that particular solver, and the lack of other values that the LFTD solver is not able to produce.

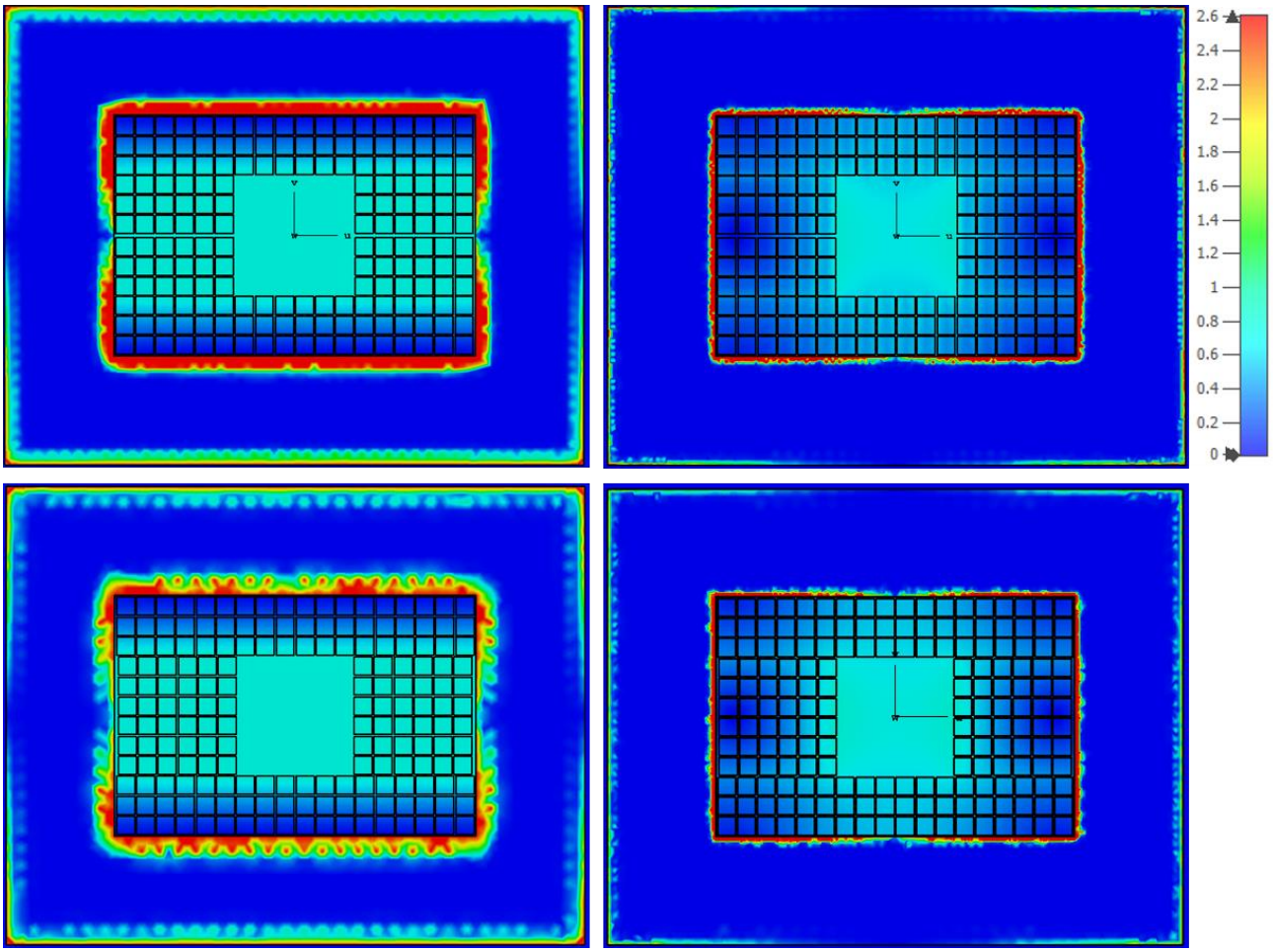

Figure 7. B-field results from CST 3D, cut plane z=0, with the real conductor (top images), idealized stranded (bottom), and between the 10 Hz (right), and 100 Hz values (left).

As can be seen in Figure 7, the slower field has more time to permeate to a greater depth of the iron whereas the faster varying is stuck in a denser patch of field close to the inner edge. Most importantly we see overall agreement between the idealized stranded and the real model.

Inductance can be calculated using the following formula derived from the stored energy of a magnet.

$$L\,[H] = \frac{2 * SE}{I^2} \tag{3}$$

Where:

SE [J] = Total stored magnetic energy, a value produced from CST.

I [A] = Total current in conductor a single conductor (2300).

Result	Idealized Stranded	Real
$B_x(0,0,0)$ [T]	0.761	0.759
$B_Y(0,0,0)$ [T]	0.710	0.676
Stored Energy [J] - X(Y)	1790 (790.1)	1779 (735.8)
Total Coil Losses [kW]	N/A	251
Total Inductance [mH] - X (Y) (Eq. 3)	0.677 (0.299)	0.673 (0.278)
Field Integral [Tcm] - X (Y)	43.7 (39.4)	43.7 (37.6)
Total Magnetic Length [cm]	57.5 (55.5)	57.6 (55.5)

Table 6. Results from 3D low frequency models.

As seen in table 6 we have good agreement between the real and idealized stranded models. The primary source of concern from this data is the total losses which come out to 251 kW. That is far from the initially calculated value of 878 kW. While less power losses is a good thing, this decreases our confidence in this value. However, upon further modeling within the low frequency time domain solver we find the same maximum value of 250 kW lost within the coils.

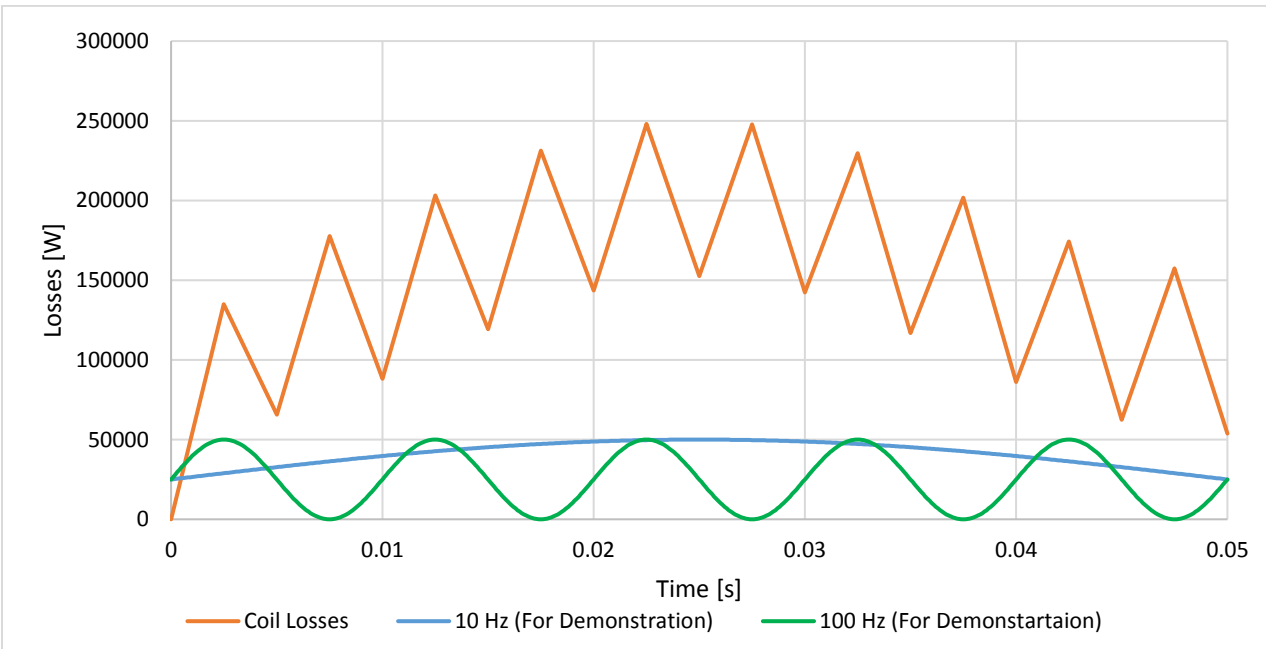

Figure 8. Total coil losses through time with representations of CST excitation signals plotted.

After molding within the time domain (Figure 8) we can see that the peak losses are at 0.025 and 0.0275 when the peak of the two exitation signals (plotted and sclaed only for demonstration). We can also see the evolution of the losses over time and how they mirror closly with the exitation signals. Again as we expected most of the losses are within the 100 Hz (Y) coils.

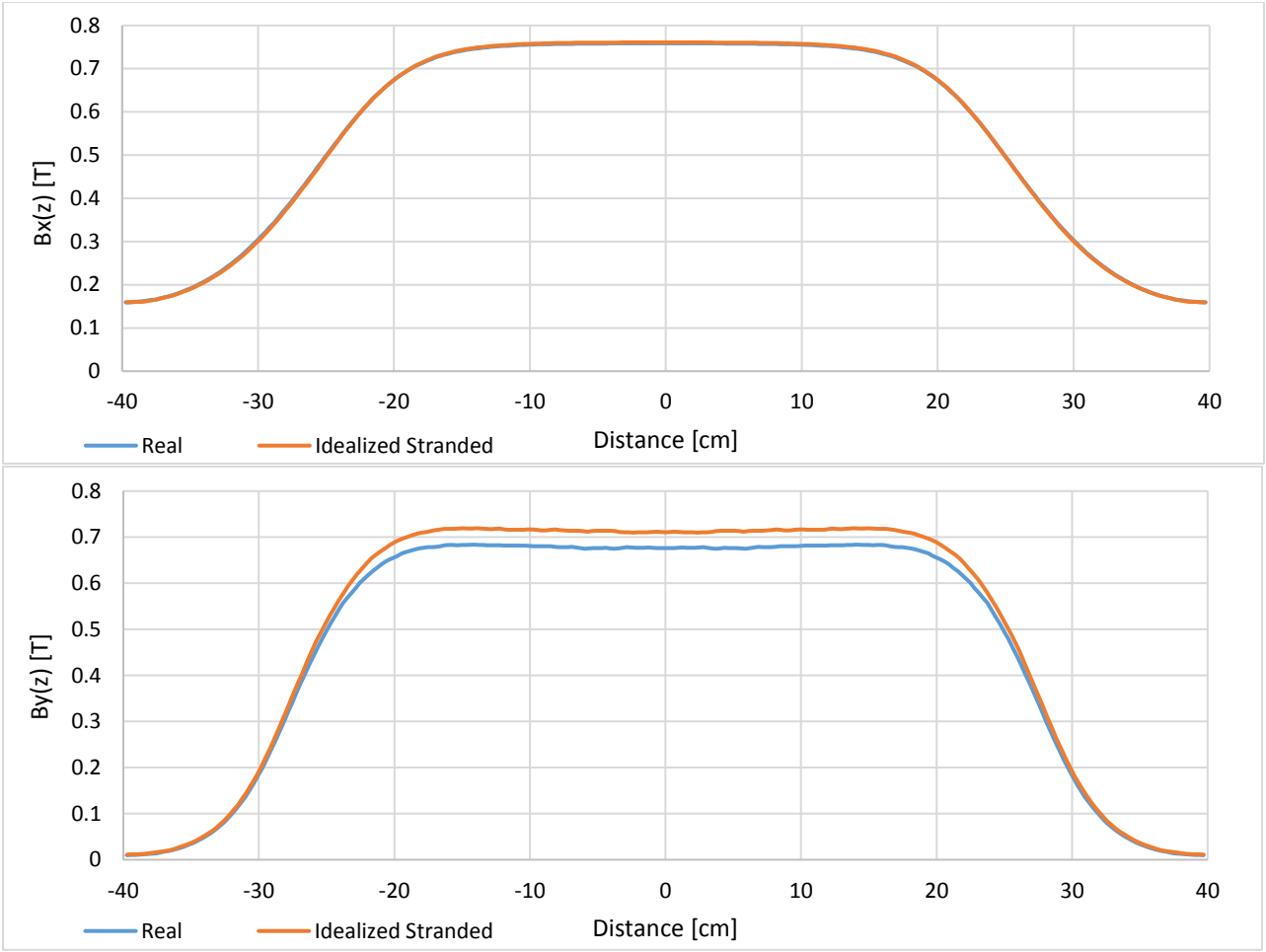

Figure 9. Bx(z) (top) and By(z) (bottom) plotted through each low frequency model.

As in the contour cross sections good agreement is seen between the two models. With a slight differentiation in the B_y field. This is believed to be a meshing issue that will go away at higher mesh values but due to hardware limitations this could not be confirmed.

Conformation Modeling

In the low frequency domain, conformation modeling was mostly done within FEMM. As in the 3D CST modeling, each frequency had to be modeled individually.

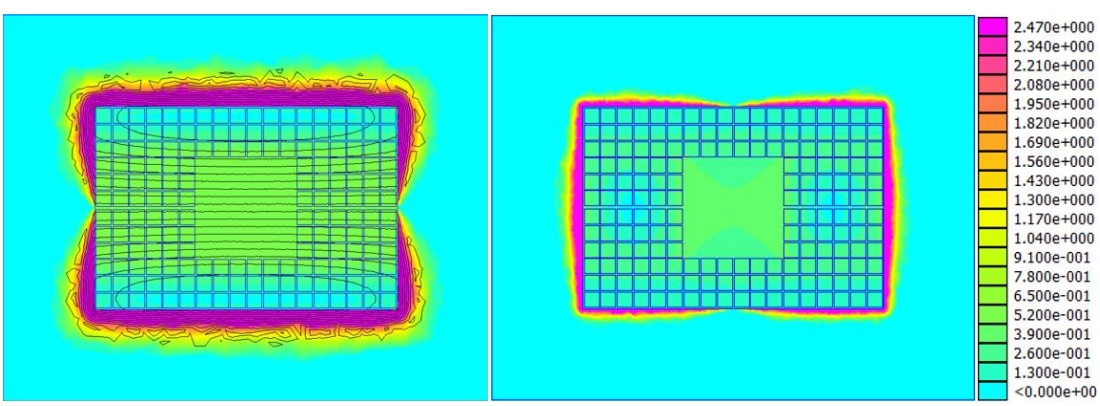

Figure 10. B-field for 10 Hz (left) and 100 Hz (left).

Again we see a very high field stuck close to the inner edge of iron with the slower field being allowed to permeate deeper into the iron and the field in the faster model having it locked in tight. This confirms the plots in Figure 7, and as seen in the static domain, the FEMM model again shows a difference in magnitude being smaller than the CST 3D computations.

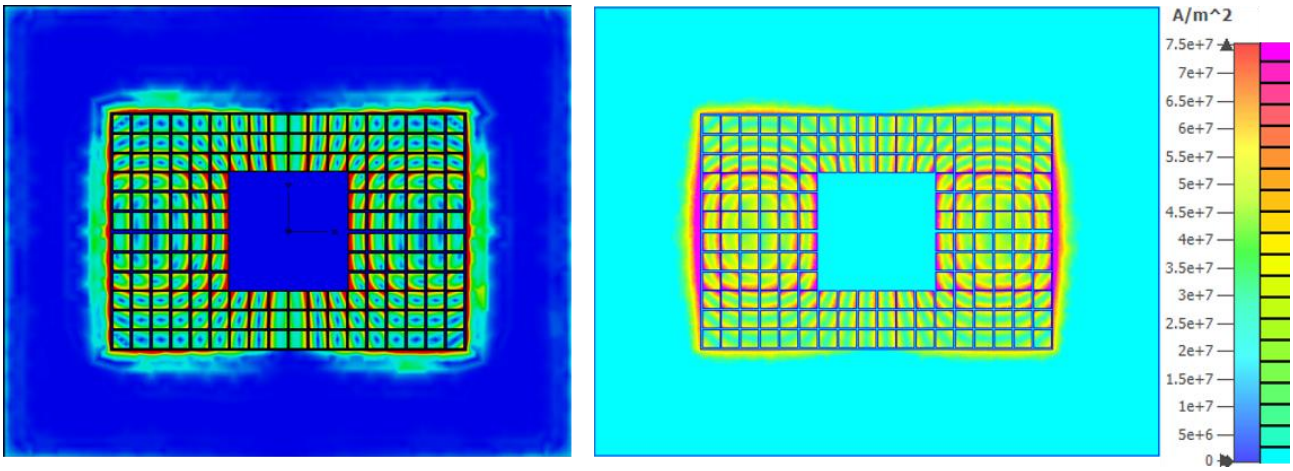

Figure 11. Maximum conductor current density for 3D CST, cut plane at z=0, (right) and 2D FEMM (left), both are at 100 Hz. Note: Only the Y (100 Hz) coil is on.

One of the most compelling agreements is when a contour plot of current density is displayed in the z=0 cutting plane. The development of almost ripple like patterns can be found in the Y (100Hz) coil in both FEMM and 3D CST.

CONCLUSIONS & FURTHER WORK

It was found that the total coil losses within these coils is expected to peak around 250 kW. Also, it was found that the alternating current will suppress the field through the aperture which must be compensated for with increasing the current.

As this project moves forward more work at much higher mesh sizes must be done while modeling the effects of iron lamination. Seeing as CST suggests that most losses are within this domain it is important that we understand if these effects will go away with the introduction of iron lamination, or if the losses are something we must design for.

Also, potential further work in optimization might be undertaken to decrease power losses, as well as further analysis on multipole components and fringe effects of the magnet.

ACKNOWLEDGMENTS

The author would like to thank his mentor, Dr. Brahim Mustapha, of the ANL Physics Division, Dr. Kathy Harkay of the ANL APS for support throughout the program, and the Lee Teng Fellowship Program.

Work supported by U. S. Department of Energy, Office of Science, under Contract No. DE-AC02-06CH11357.

REFERENCES

[1] V. Anferov, "Combined X-Y sanning magnet ffor conformal proton radiation thearpy," *Medical Physics,* vol. 32, no. 3, pp. 815-818, 2005.

[2] L. Marks, "Conventional magnets -II," Daresbury Laboratory, Warrington.

[3] D. C. Meeker, *Finite Element Method Magnetics,* Version 4.2 (28Feb2018 Build) ed. http://www.femm.info

[4] B. Mustapha and a. et., "Prospects for an advanced heavy ion therapy center in the chicago area," US Department of Energy, Chicago, 2018.